isvr Institute of Sound and Vibration Research

Robust Control of Subzero III In Restricted Water

Z. Feng and R. Allen

ISVR Technical Memorandum 926

November 2003

University of Southampton

SCIENTIFIC PUBLICATIONS BY THE ISVR

Technical Reports are published to promote timely dissemination of research results by ISVR personnel. This medium permits more detailed presentation than is usually acceptable for scientific journals. Responsibility for both the content and any opinions expressed rests entirely with the author(s).

Technical Memoranda are produced to enable the early or preliminary release of information by ISVR personnel where such release is deemed to the appropriate. Information contained in these memoranda may be incomplete, or form part of a continuing programme; this should be borne in mind when using or quoting from these documents.

Contract Reports are produced to record the results of scientific work carried out for sponsors, under contract. The ISVR treats these reports as confidential to sponsors and does not make them available for general circulation. Individual sponsors may, however, authorize subsequent release of the material.

UNIVERSITY OF SOUTHAMPTON

INSTITUTE OF SOUND AND VIBRATION RESEARCH

SIGNAL PROCESSING & CONTROL GROUP

Robust Control of Subzero III in Restricted Water

by

Z.Feng and R.Allen

ISVR Technical Memorandum N° 926

November 2003

Authorised for issue by
Prof S J Elliott
Group Chairman

Contents

1 Introduction.....1
2 Reduced-order H∞ control synthesis.....1
2.1 Problem formulation.....1
2.2 The TMP-based design approach.....2
2.3 Trade-off between the controller order and the performance.....3
3 Redesign of the heading autopilot.....5
3.1 Reduction of overshoot.....5
3.2 Reduction of control effort 8
3.3 The MISO control scheme..... 10
4 Redesign of longitudinal autopilot.....14
4.1 Redesign of the speed autopilot.....14
4.2 Redesign of the depth autopilot.....15
5 Conclusions.....18
References.....19

1 Introduction

In previous reports (Feng and Allen, 2002), we presented the design of H_∞ autopilots and reduced-order H_∞ autopilots for Subzero III. Since the vehicle was not ready for water trails at that time, only simulation results were given. Whether these robust autopilots are valid for the real vehicle remains unknown.

Lots of practical work has been undertaken since the presentation of vehicle on the 1st IFAC Conference on Guidance and Control of Underwater Vehicles, Newport, 9-11 April 2003. The technicians in ISVR of Southampton University refined the software running in the onboard MCU and upgraded the hardware including the sensors for feedback control. In addition the control program running in the MATLAB® environment of the control computer on the shore was also enhanced to enable joystick operation and allow system identification and control tests to be carried out.

The vehicle was ready for testing in May 2003. Due to its low cost and availability, the Lamont Towing Tank of Southampton University was chosen as the venue for water trails. The tank has a length of 30m, a width of 2.4m and a depth of 1.2m. It was soon found that the tank is not well suited for water tests of an underwater flight vehicle equipped with the autopilots that were designed for open water flight control since the vehicle can hit the sidewalls or the bottom of the tank during water trails. The restricted size of the Lamont tank presents a big challenge for the control of Subzero III.

To enable the vehicle to track demanded heading and depth with tolerant overshoot, the robust autopilots for the flight control of Subzero III were redesigned. Moreover the control effort is also considered in the design to save the on-board power consumption.

This report presents the redesign of the robust autopilots for the flight control of Subzero III in the restricted size of the Lamont tank and presents results from the water trials. In section 2, the design method for synthesizing reduced-order H_∞ controller is introduced. The redesign of the heading and the longitudinal autopilots is presented in sections 3 and 4, respectively. Finally some concluding remarks are given in section 5.

2 Reduced-order H_∞ control synthesis

2.1 Problem formulation

Given a generalized plant model

$$\begin{aligned} \dot{x} &= Ax + B_1 w + B_2 u \\ z &= C_1 x + D_{11} w + D_{12} u \\ y &= C_2 x + D_{21} w \end{aligned} \tag{1}$$

where $w \in R^{m_1}$ is the external input vector, $u \in R^{m_2}$ the control input vector, $z \in R^{p_1}$ the controlled output vector, $y \in R^{p_2}$ the measurement vector, $x \in R^n$ the state vector.

The reduced-order or low-order H_∞ control problem is to find an output feedback controller $u=K(s)\,y$ of order $k<n$ such that: 1) the closed-loop system is internally stable; and 2) the l_2-gain of the closed-loop system is strictly less than the prescribed level γ, i.e. $\|T_{zw}(s)\|_\infty < \gamma$, where $T_{zw}(s)$ is the closed-loop transfer function from w to z.

Define the following three convex sets:

$$L_X(\gamma) := \left\{ X \in R^{n\times n} : X = X^T > 0, \begin{bmatrix} S^T & 0 \\ 0 & I \end{bmatrix} \begin{bmatrix} AX + XA^T & XC_1^T & B_1 \\ C_1X & -\gamma I & D_{11} \\ B_1^T & D_{11}^T & -\gamma I \end{bmatrix} \begin{bmatrix} S & 0 \\ 0 & I \end{bmatrix} < 0 \right\}$$

$$L_Y(\gamma) := \left\{ Y \in R^{n\times n} : Y = Y^T > 0, \begin{bmatrix} W^T & 0 \\ 0 & I \end{bmatrix} \begin{bmatrix} A^TY + YA & YB_1 & C_1^T \\ B_1^TY & -\gamma I & D_{11}^T \\ C_1 & D_{11} & -\gamma I \end{bmatrix} \begin{bmatrix} W & 0 \\ 0 & I \end{bmatrix} < 0 \right\}$$

$$L(\gamma) := \{ (X,Y) : X \in L_X(\gamma), Y \in L_Y(\gamma), \begin{bmatrix} X & I \\ I & Y \end{bmatrix} \geq 0 \}$$

where the columns of W and S form the bases of the null spaces of $\begin{bmatrix} C_2 & D_{21} \end{bmatrix}$ and $\begin{bmatrix} B_2^T & D_{12}^T \end{bmatrix}$, respectively.

It is well known that reduced-order H_∞ control problem is indeed a rank minimization problem (RMP) over the convex set $L(\gamma)$ (see El Ghaoui et al 1993, Gahinet et al 1994 and Iwasaki et al 1994), i.e.

$$\rho(\gamma) = \arg\min_{(X,Y)\in L(\gamma)} \mathrm{Rank} \begin{bmatrix} X & I \\ I & Y \end{bmatrix} \tag{2}$$

If $L(\gamma)$ is not empty, then the RMP(2) admits an extreme $\rho^*(\gamma)$ and the resulting controller has an order $k = \rho^*(\gamma) - n$. Obviously, a reduced-order controller exists when $\rho^*(\gamma) < 2n$.

Although $L(\gamma)$ is convex, the RMP(2) is difficult to solve due to the non-convex objective. By relaxing the minimization of the rank of a positive semi-definite matrix to the minimization of its trace, the RMP(2) is approximated by the trace minimization problem (TMP):

$$J(\gamma) = \arg\min_{(X,Y)\in L(\gamma)} \mathrm{Trace} \begin{bmatrix} X & I \\ I & Y \end{bmatrix} \tag{3}$$

Although the RMP (2) and the TMP (3) are not equivalent since the former minimizes the number of the non-zero singular values of a symmetric and positive semi-definite matrix while the latter minimizes the sum of its non-zero singular values, it is a well known fact that the TMP (3) tends to yield a low-rank solution, i.e. a few of the singular values tends to zero.

A design approach based upon the TMP (3) is given in the next section.

2.2 The TMP-based design approach

1) Solve the TMP(3).

If the pair (X^*, Y^*) solves the TMP (3), and $(n-k)$ singular values of $(Y^* - X^{*-1})$ tend to zero (very small), then the reduced-order H_∞ controller of k^{th} order exists. The reduced-order controller can be obtained via the remaining steps.

2) Construct a $(n+k)\times(n+k)$ symmetric positive definite matrix

$$P = \begin{bmatrix} Y^* & U\Sigma^{1/2} \\ \Sigma^{1/2}U^T & I_{k\times k} \end{bmatrix}$$

where $\Sigma = \mathrm{diag}(\sigma_1, \cdots, \sigma_k)$ and $U \in R^{n\times k}$ are obtained from the singular value decomposition of $(Y^* - X^{*-1})$ with $\sigma_i (i = 1, \cdots, k)$ being the non-zero singular values in the descending order and U satisfying $U^T U = I_{k\times k}$ and

$$UU^T = \begin{bmatrix} I_{k\times k} & 0_{k\times(n-k)} \\ 0_{(n-k)\times k} & 0_{(n-k)\times(n-k)} \end{bmatrix}$$

3) Solve the LMI in $G \in R^{(k+m_2)\times(k+m_2)}$ (see Gahinet et al 1994)

$$\Phi + \Omega^T G \Psi + \Psi^T G^T \Omega < 0$$

where

$$\Phi = \begin{bmatrix} P\hat{A} + \hat{A}^T P & P\hat{B}_1 & \hat{C}_1^T \\ \hat{B}_1^T P & -\gamma I & D_{11}^T \\ \hat{C}_1 & D_{11} & -\gamma I \end{bmatrix} \quad \Omega = \begin{bmatrix} \hat{B}_2^T P & 0 & \hat{D}_{12}^T \end{bmatrix}$$

$$\Psi = \begin{bmatrix} \hat{C}_2 & \hat{D}_{21} & 0 \end{bmatrix}$$

with

$$\hat{A} = \begin{bmatrix} A & 0_{n\times k} \\ 0_{k\times n} & 0_{k\times k} \end{bmatrix}, \hat{B}_2 = \begin{bmatrix} 0_{n\times k} & B_2 \\ I_{k\times k} & 0_{k\times m_2} \end{bmatrix}, \hat{C}_2 = \begin{bmatrix} 0_{k\times n} & I_{k\times k} \\ C_2 & 0_{p_2\times k} \end{bmatrix}, \hat{B}_1 = \begin{bmatrix} B_1 \\ 0_{k\times m_1} \end{bmatrix},$$

$$\hat{C}_1 = \begin{bmatrix} C_1 & 0_{p_1\times k} \end{bmatrix}, \hat{D}_{12} = \begin{bmatrix} 0_{p_1\times k} & D_{12} \end{bmatrix}, \hat{D}_{21} = \begin{bmatrix} 0_{k\times m_1} \\ D_{21} \end{bmatrix}$$

An alternative way to obtain G is to apply the explicit formulas given by Iwasaki and Skelton (1994).

4) Obtain a realization of the controller from G. This is achieved by partitioning G into four blocks as

$$G = \begin{bmatrix} G_{11} & G_{12} \\ G_{21} & G_{22} \end{bmatrix}$$

with $G_{11} \in R^{k\times k}, G_{12} \in R^{k\times p_2}, G_{21} \in R^{m_2\times k}$ and $G_{22} \in R^{m_2\times p_2}$. And a state space realization of the controller can be selected as $(G_{11}, G_{12}, G_{21}, G_{22})$.

Before the TMP-based approach is applied to the design of reduced-order autopilots for Subzero III, a theoretical insight into the trade-off between the controller order and the performance of the closed-loop system will be given.

2.3 Trade-off between the controller order and the performance

As illustrated by the examples in Pare and How (1999) and Fazel (2002), the controller order and the performance of the closed-loop system are two contradicting

design specifications. Consequently a trade-off needs to be made between them. As stated in Theorem 1, a theoretical insight into this trade-off is given in this section.

Theorem 1 If $L(\gamma)$ is non-empty, then $L(\gamma+\Delta\gamma)$ is non-empty and $L(\gamma)\subseteq L(\gamma+\Delta\gamma)$ for any $\Delta\gamma>0$.

Proof Supposing $(X,Y)\in L(\gamma)$, it suffices to check if $(X,Y)\in L(\gamma+\Delta\gamma)$ for any $\Delta\gamma>0$. This can then be reduced to checking if $X\in L_X(\gamma+\Delta\gamma)$ and $Y\in L_Y(\gamma+\Delta\gamma)$ in terms of the definition of $L(\gamma)$.

For any $\Delta\gamma>0$, one has

$$\begin{bmatrix} S^T & 0 \\ 0 & I \end{bmatrix}\begin{bmatrix} AX+XA^T & XC_1^T & B_1 \\ C_1X & -(\gamma+\Delta\gamma)I & D_{11} \\ B_1^T & D_{11}^T & -(\gamma+\Delta\gamma)I \end{bmatrix}\begin{bmatrix} S & 0 \\ 0 & I \end{bmatrix}$$

$$=\begin{bmatrix} S^T & 0 \\ 0 & I \end{bmatrix}\begin{bmatrix} AX+XA^T & XC_1^T & B_1 \\ C_1X & -\gamma I & D_{11} \\ B_1^T & D_{11}^T & -\gamma I \end{bmatrix}\begin{bmatrix} S & 0 \\ 0 & I \end{bmatrix}+\begin{bmatrix} S^T & 0 \\ 0 & I \end{bmatrix}\begin{bmatrix} 0 & 0 & 0 \\ 0 & -\Delta\gamma I & 0 \\ 0 & 0 & -\Delta\gamma I \end{bmatrix}\begin{bmatrix} S & 0 \\ 0 & I \end{bmatrix}$$

The first term on the right hand side is negative definite since it is supposed that $X\in L_X(\gamma)$, and the second term on the right hand side is negative semi-definite due to positive $\Delta\gamma$. Therefore the right hand side is negative definite, i.e. $X\in L_X(\gamma+\Delta\gamma)$. Similarly, it can be shown that $Y\in L_Y(\gamma+\Delta\gamma)$.

This concludes the proof.

Corollary The objective of any optimization within $L(\gamma)$ will either be improved or invariant as γ increases.

This is because the feasible set $L(\gamma)$ within which the optimal value of objective functions is sought is expanding as performance level γ increases. Therefore for the RMP (2), we have

$$\rho^*(\gamma+\Delta\gamma)\le\rho^*(\gamma),\quad\forall\Delta\gamma>0 \tag{4}$$

and for the TMP (3), we have

$$J^*(\gamma+\Delta\gamma)\le J^*(\gamma),\quad\forall\Delta\gamma>0 \tag{5}$$

It should be noted that while reducing the order or the trace of the positive semi-definite matrix (if this is possible) always requires the performance to degrade, sacrificing the performance does not necessarily guarantee to generate improved objectives for the RMP (2) or the TMP (3). In other words, as performance level γ increases to a certain value, the RMP (2) or TMP (3) will not be improved any more. This suggests that to increase the performance γ level from its optimal value γ^* gradually and check if the controller order is reduced by applying the TMP(3).

The optimal H_∞ performance level γ^* can be determined by the convex programming

$$\gamma^*=\arg\min_{(X,Y)\in L(\gamma)}\gamma \tag{6}$$

An efficient way to solve this problem is to use off-shelf software packages e.g. the LMI Toolbox in Matlab.

3 Redesign of the heading autopilot

3.1 Reduction of overshoot

The robust control of the vehicle is interpreted as the mixed-sensitivity optimization problem as depicted in Figure 1, where $G(s)$ is the nominal model of the vehicle around the cruising condition (straight ahead motion with a constant speed of 1.3 m/s), $K(s)$ is the autopilot to be designed, the weighting functions $W_1(s), W_2(s)$ and $W_3(s)$ penalize the tracking error, control effort and modelling error, respectively.

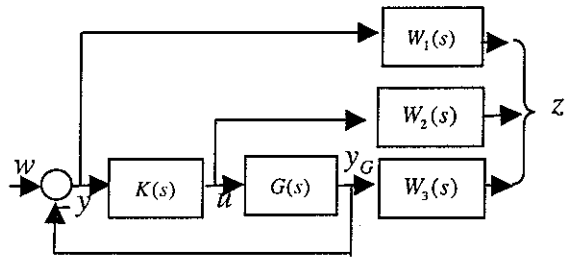

Figure 1. The robust control system

For heading control, $G(s)$ is the transfer function from the rudder command to the heading, $K(s)$ is the heading autopilot, and $W_1(s)$, $W_2(s)$ and $W_3(s)$ penalize the heading error, rudder deflection, and the model uncertainty of the heading system, respectively.

For depth control, $G(s)$ is the transfer function from the stern-plane command to the depth, $K(s)$ is the depth autopilot, and $W_1(s)$, $W_2(s)$ and $W_3(s)$ punish the depth error, deflection of the stern-planes, and the model uncertainty of the depth system, respectively.

For forward speed control, $G(s)$ is the transfer function from the propeller command to the forward speed, $K(s)$ is the speed autopilot, and $W_1(s)$, $W_2(s)$ and $W_3(s)$ punish the speed error, propeller command and modelling error of the speed system, respectively.

Here we consider the heading control only. The depth and speed control will be discussed in the next section.

It was found that the overshoot in the heading was so large that the vehicle hit the tank's sidewall when we tried to verify the heading autopilot presented in the previous report. Whether or not the old autopilot is valid in open water with a much larger manoeuvrability space still needs to be checked in future.

For the vehicle to have the ability of course-keeping in the restricted water, it is obviously necessary to restrict the overshoot of the vehicle's heading.

In the frame of mixed-sensitivity optimization, this can only be done by adjusting the three weighting functions since the nominal model is a fixed part in Figure 1.

Since $W_1(s)$ can only affect the steady state performance, it is chosen the same as in the old design, i.e.

$$W_1(s) = \frac{10(s+10)}{1000s+1} \tag{7}$$

which restricts the steady state error to be below the level of 1% .

Therefore we can only modify the other two weighting functions. To reduce the heading overshoot, which is a dynamic performance index, as much as possible, one conservative way is to gain maximal rudder manoeuvrability. This can be achieved simply setting

$$W_2(s) = 0 \tag{8}$$

which means the rudder efforts is only restricted physically by the servo mechanism.

However the choice (8) can only guarantee the dynamic performance, which is a combination of overshoot and settling time of the closed-loop system under a step reference, to be improved. To fully utilize the control effort to restrict the overshoot, it is necessary to modify the design of the weighting function $W_3(s)$.

In the frame of mixed-sensitivity optimisation, the choice of $W_3(s)$ usually depends on the requirement on the attenuation in the high frequency region where the model uncertainty occurs. This implies that one has a freedom to modify its characteristics in low frequency region.

As presented by Hu et al (2000), by approximating the closed-loop system with a typical second-order system, the restriction on the magnitude of the closed-loop transfer function is determined by

$$\left|T(jw)\right|_{\max} \le -\frac{\pi^2 + \log^2 e_{\max}}{2\pi \log e_{\max}}$$

in the low frequency region, where $e_{\max}$ is the percentage maximum overshoot.

Therefore in terms of the above inequality to confine the overshoot smaller than 10%, $\left|T(jw)\right|_{\max} \le 1.0487$ must be guaranteed. To combine this requirement with the attenuation rate of -40 dB/Dec to high frequency model uncertainty, the weighting function $W_3(s)$ is selected as

$$W_3(s) = \frac{(s+14.33)^2}{215.34} \tag{9}$$

By augmenting the plant dynamics with the weighting functions, the generalized plant model can be obtained as

$$P(s) = \left[\begin{array}{c|c} W_1(s) & -W_1(s)G(s) \\ 0 & W_3(s)G(s) \\ \hline I & -G(s) \end{array}\right] \tag{10}$$

Denote the state-space realizations of $G(s)$ and $W_1(s)$ by (A_G, B_G, C_G, D_G) and $(A_{W_1}, B_{W_1}, C_{W_1}, D_{W_1})$, a state-space realization of $P(s)$ can be obtained as follows (cf. Eq. (1)).

$$\left[\begin{array}{c|c|c} A & B_1 & B_2 \\ \hline C_1 & D_{11} & D_{12} \\ \hline C_2 & D_{21} & D_{22} \end{array}\right] = \left[\begin{array}{cc|c|c} A_G & 0 & 0 & B_G \\ -B_{W_1}C_G & A_{W_1} & B_{W_1} & -B_{W_1}D_G \\ \hline -D_{W_1}C_G & C_{W_1} & D_{W_1} & -D_{W_1}D_G \\ \tilde{C} & 0 & 0 & \tilde{D} \\ \hline -C_G & 0 & I & -D_G \end{array}\right] \tag{11}$$

where

$$\Pi_0 + s\Pi_1 + s^2\Pi_2 = W_3(s)$$

$$\tilde{C} = \Pi_0 C_G + \Pi_1 C_G A_G + \Pi_2 C_G A_G^2$$

$$\tilde{D} = \Pi_0 D_G + \Pi_1 C_G B_G + \Pi_2 C_G A_G B_G$$

Due to the passive stability of the roll mode, the state space model of the heading system around the cruise condition is reduced to

$$\dot{x}_G = A_G x_G + B_G u, y_G = C_G x + D_G u \tag{12}$$

where the state, control input and output are

$$x_G = [\psi, v, r, \delta r]^T, u = \delta r_d, y_G = \psi \tag{13}$$

and the state space model can be obtained by linearizing the non-linear model around the cruise condition,

$$G(s) = \left[\begin{array}{c|c} A_G & B_G \\ \hline C_G & D_G \end{array}\right] = \left[\begin{array}{cccc|c} 0 & 0 & 1 & 0 & 0 \\ 0 & -2.126 & 0.3733 & 0.22 & 0 \\ 0 & 7.994 & -8.703 & -1.623 & 0 \\ 0 & 0 & 0 & -7.69 & 1 \\ \hline 57.3 & 0 & 0 & 0 & 0 \end{array}\right] \tag{14}$$

Inserting the plant model (14) and the weighting functions (7)-(9) into (11), a generalized plant model of 5th order can be determined. By substituting this model into (1) and invoking the reduced-order H_∞ design approach in section 2, a 3rd heading autopilot with the H_∞ performance of 0.9633 can be obtained. The transfer function of the heading autopilot is

$$K_\psi^1(s) = \frac{-97.0346(s+0.03386)(s^2+6.124s+14.99)}{(s+0.001164)(s+93.28)(s+2.639)} \tag{15}$$

The frequency responses of the sensitivity function and the complementary sensitivity function are plotted in Figure 2.

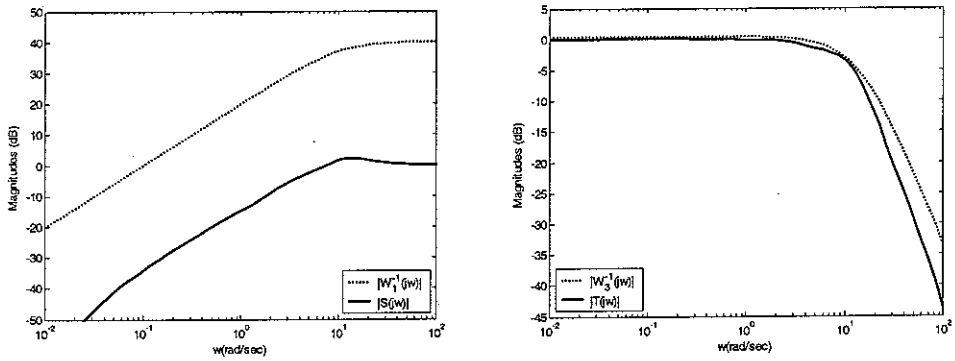

Figure 2. The frequency response of sensitivity function (left) and the complementary sensitivity function (right)

From Figure 2, it can be seen that the design objective of the mixed-sensitivity optimization is achieved.

Equipped with the heading autopilot (15), the vehicle was then tested in the Lamont Tank to verify the ability of course-keeping. It should be noted here that while the heading was controlled in closed loop, the forward speed and depth were controlled in open-loop manner.

Although the heading autopilot was deigned for the cruise condition (straight ahead motion with constant speed of 1.3m/s), it was tested under the off-nominal condition, i.e. the vehicle accelerated from stationary to a speed which may not be the cruise speed, since it is very difficult to build the nominal condition prior to the nominal test

in the restricted water of the tank. This did present a challenge for the robustness of the heading autopilot due to the model uncertainty.

The heading autopilot was tested by setting the vehicle's initial heading to a direction different from the desired direction which is parallel to the sidewalls of the tank.

By giving the propeller a step command which corresponds to a final speed of about 1m/s, and adjusting the stern-planes via the joystick to roughly keep a depth, the heading was controlled by the heading autopilot while the vehicle was moving forward. It was seen that the vehicle could track the desired direction with a small lateral displacement. A test result collected on 15th August 2003 is shown in Figure 3.

It can clearly be seen that the vehicle's heading converges to the desired direction within six seconds. So from the test result, we can conclude that the redesign of the heading autopilot is successful in reducing the overshoot of heading for the flight control of Subzero III in the restricted water. Moreover the heading autopilot is robust to model uncertainty since it worked well under off-nominal operating conditions.

However, the rudder command is frequently truncated by the saturation limit of the rudder. This means the rudder is almost switching between its two limit positions to provide maximal manoeuvrability. This is not desirable from the viewpoint of power consumption and actuator longevity which is critical for an autonomous underwater vehicle.

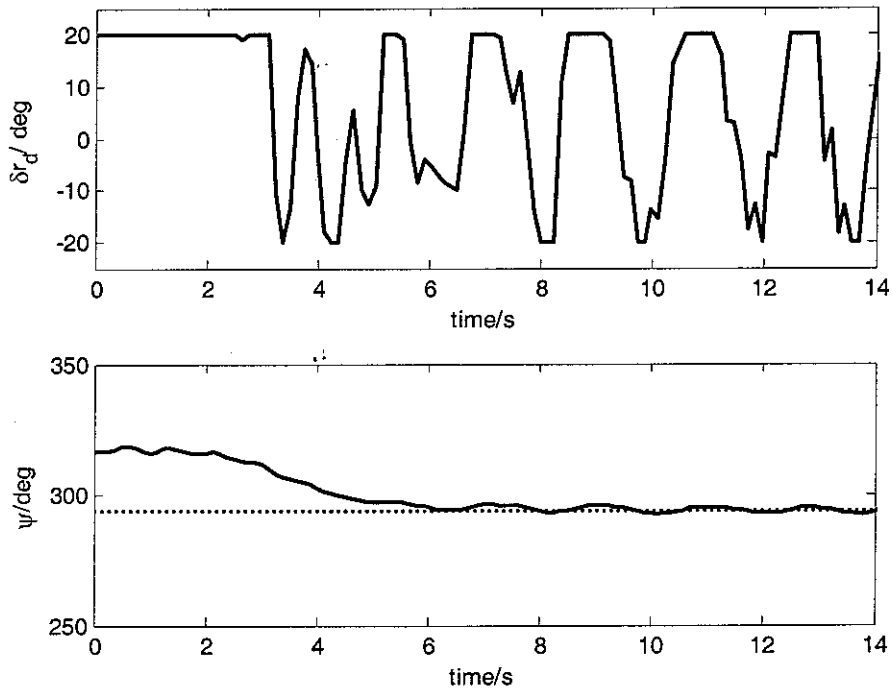

Figure 3 Test result of heading control.
Upper: rudder command, bottom: actual heading (solid) and demanded heading (dotted)

3.2 Reduction of control effort

To save the power consumption, a natural way in the frame of mixed-sensitivity optimization is to reflect the requirement on control effort in the weighting function $W_2(s)$. This idea is utilized here to redesign the heading autopilot.

Neglecting the hysteresis of the rudder, it is simplified as a nonlinearity of saturation with a limit of 20 degrees, i.e. $|\delta r_d| \le 20^o$.

In the new design, the weighting function is selected as

$$W_2(s) = W_2 = 2 \tag{16}$$

This means the rudder command will be less than 0.5° for a 1° step of heading demand. Or equivalently, the rudder command will be less than the saturation limit of 20° for the heading step of a magnitude less than 40°.

By replacing the generalized plant (10) with

$$P(s) = \left[\begin{array}{c|c} W_1(s) & -W_1(s)G(s) \\ 0 & W_2(s) \\ 0 & W_3(s)G(s) \\ \hline I & -G(s) \end{array}\right] \tag{17}$$

Substituting (7), (9), (14) and (16) into (17) yields the generalized plant. The minimal realization of this transfer function is

$$\left[\begin{array}{c|c|c} A & B_1 & B_2 \\ \hline C_1 & D_{11} & D_{12} \\ \hline C_2 & D_{21} & D_{22} \end{array}\right] = \left[\begin{array}{cc|c|c} A_G & 0 & 0 & B_G \\ -B_{W_1}C_G & A_{W_1} & B_{W_1} & -B_{W_1}D_G \\ \hline -D_{W_1}C_G & C_{W_1} & D_{W_1} & -D_{W_1}D_G \\ 0 & 0 & 0 & W_2 \\ \tilde{C} & 0 & 0 & \tilde{D} \\ \hline -C_G & 0 & I & -D_G \end{array}\right] \tag{18}$$

Again by inserting (18) into (1) and applying the design approach in section 2, a heading autopilot of 3rd order with H_∞ performance of 0.9978 can be obtained. Its transfer function is

$$K_\psi^2(s) = \frac{-0.47118(s+4.733)(s+1.803)(s+0.006352)}{(s+5.721)(s+1.406)(s+0.001001)} \tag{19}$$

The frequency responses of the sensitivity function, complementary sensitivity function and the control effort of the closed-loop system are shown in Figure 4.

From Figure 4, it can be seen that the design objective of the mixed-sensitivity optimization is achieved.

Again the heading autopilot (19) was then tested for off-nominal conditions in the Lamont Tank to verify the ability of course keeping. The test configuration is the same as described earlier.

A test result collected on 22nd October 2003 is shown in Figure 5. It can be seen that while the rudder effort is reduced significantly (cf. Figure 4), the tracking performance is obviously degraded due to its large overshoot as well as the oscillations of large magnitudes at the final stage.

Therefore the dynamic performance of the heading control system still needs to be improved.

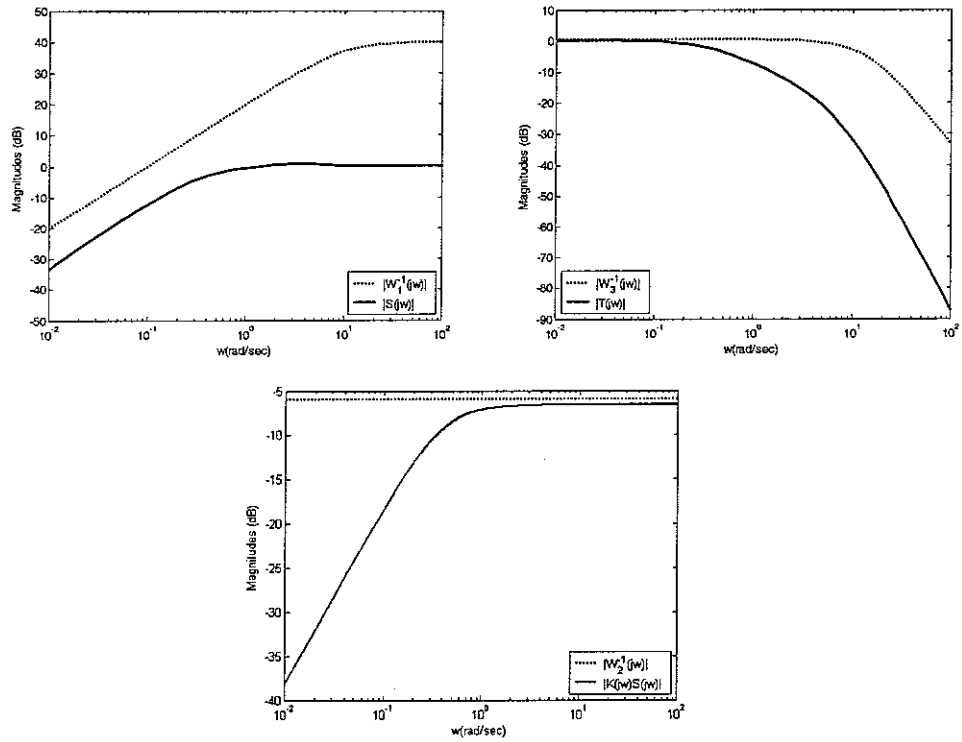

Figure 4. The frequency responses of the closed-loop system
Upper left: the sensitivity function, upper right: the complementary sensitivity function, bottom: the control effort

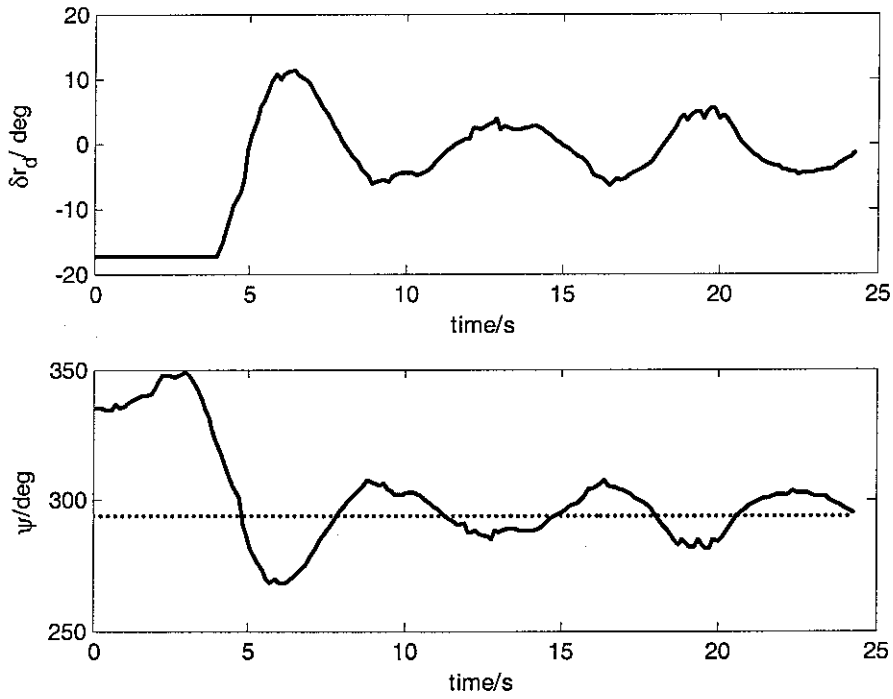

Figure 5. Test result of heading control.
Upper: rudder command, bottom: actual heading (solid) and demanded heading (dotted)

3.3 The MISO control scheme

In the last two sections, the heading autopilots that feed the output (heading measurement) were designed. They are both single-input single-output controller.

The two schemes are not desirable, the first autopilot cost two much onboard power, while the second has a very poor dynamic performance. In this section, as illustrated in Figure 6, a new scheme is presented.

As shown in Figure 6, the heading autopilot (enclosed by the dashed lines) is a MISO (multiple-input single-output) system, i.e. it has the heading error e_ψ and the yaw rate r as its input and the rudder command δr_d as its output. The introduction of the yaw rate to the feedback channel is based upon the idea that feedback of the output's rate can improve the dynamic performance.

Since for underwater vehicles that move in six degrees of freedom, we have

$$\dot{\psi} = q\frac{\sin\phi}{\cos\theta} + r\frac{\cos\phi}{\cos\theta}$$

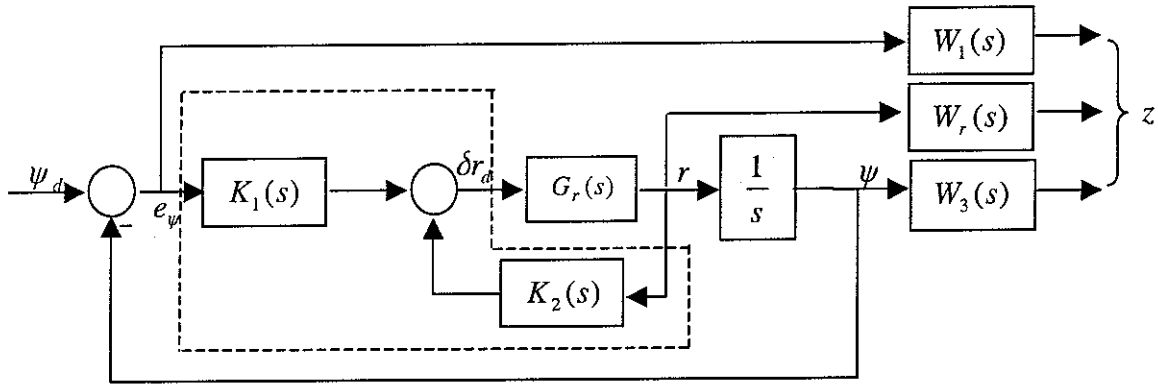

Figure 6. The MISO robust heading control system

Thus for an underwater vehicle whose roll modes are passively stable, we have

$$\dot{\psi} \approx \frac{r}{\cos\theta}$$

Moreover for an underwater flight vehicle that is moving ahead with small pitch angles, we have

$$\dot{\psi} \approx r$$

Therefore

$$G(s) = \frac{1}{s}G_r(s) \tag{19}$$

where $G_r(s)$ denoting the transfer function from the rudder command to the yaw rate.

Selecting the state, the control input and the output as

$$\dot{x}_r = [v, r, \delta r]^T, u_r = \delta r_d, y_r = r$$

the realization of $G_r(s)$ can be obtained as

$$G_r(s) = \left[\begin{array}{c|c} A_r & B_r \\ \hline C_r & D_r \end{array}\right] = \left[\begin{array}{ccc|c} -2.134 & 0.3697 & 0.2175 & 0 \\ 7.963 & -8.717 & -1.633 & 0 \\ 0 & 0 & -7.69 & 1 \\ \hline 0 & 1 & 0 & 0 \end{array}\right] \tag{20}$$

Besides the difference in the structure of the heading autopilot, the controlled output z is also different from the previous schemes. In the new scheme, the yaw rate instead of the rudder command is penalized. The reason for this modification is while penalizing the rudder command is only an indirect way to restrict the control effort (the rudder deflection) since the actuator (rudder) has its own dynamics, confining the

yaw rate is a direct way to restrict the control effort since it directly reflects the rudder position (not the rudder command).

In the new scheme, the new weighting function $W_r(s)$ is selected as

$$W_r(s) = W_r = 2 \tag{21}$$

which means the yaw rate needs to be less than 0.5°/s for a 1° step of heading demand. In other words, the yaw rate will be less than 5°/s for a 10° step of heading demand.

By setting the external input, control input, the measurement and the controlled output as

$$w = \psi_d, u = \delta r_d, y = [e_\psi, r]^T, z = [W_1 e_\psi, W_r r, W_3 \psi]^T$$

the transfer function of the generalized plant can be described by

$$P(s) = \left[\begin{array}{c|c} W_1(s) & -W_1(s)G(s) \\ 0 & W_r(s)G_r(s) \\ 0 & W_3(s)G(s) \\ \hline I & -G(s) \\ 0 & G_r(s) \end{array}\right] \tag{22}$$

The autopilot to be devised can be described as

$$K(s) = [K_1(s) \quad K_2(s)]$$

A minimal realization of $P(s)$ is

$$\left[\begin{array}{c|c|c} A & B_1 & B_2 \\ \hline C_1 & D_{11} & D_{12} \\ \hline C_2 & D_{21} & D_{22} \end{array}\right] = \left[\begin{array}{ccc|c|c} A_{W_1} & -B_{W_1} & 0 & B_{W_1} & 0 \\ 0 & 0 & C_r & 0 & D_r \\ 0 & 0 & A_r & 0 & B_r \\ \hline C_{W_1} & -D_{W_1} & 0 & D_{W_1} & 0 \\ 0 & 0 & W_r C_r & 0 & W_r D_r \\ 0 & \Pi_0 & \Pi_1 C_r + \Pi_2 C_r A_r & 0 & \Pi_1 D_r + \Pi_2 C_r B_r \\ \hline 0 & -1 & 0 & 1 & 0 \\ 0 & 0 & C_r & 0 & D_r \end{array}\right] \tag{23}$$

Inserting (23) into (1) and using the design approach in section 2, a 2nd order autopilot with H_∞ performance of 0.9984. The transfer function of the autopilot is

$$K_\psi^3(s) = \left[\frac{-6.5659(s+8.362)(s+0.004654)}{(s+0.6485)(s+0.0008644)} \quad \frac{15.0138(s+6.54)(s+0.0002916)}{(s+0.6485)(s+0.0008644)}\right] \tag{24}$$

The frequency responses of the sensitivity function, complementary sensitivity function of heading control system and the closed-loop yaw rate system are shown in Figure 6.

Again from Figure 6, it can be seen that all the design specifications are satisfied.

The heading autopilot was then tried in the off-nominal tests. A test result is plotted in Figure 7. Form Figure 7, it can be seen the rudder effort is reasonable and the tracking performance of the heading is significantly improved (cf. Figures 3 and 5).

Note that during the test, the yaw rate is calculated from the numerical difference of the heading angle since the yaw rate given by the rate gyro was too noisy to be useful.

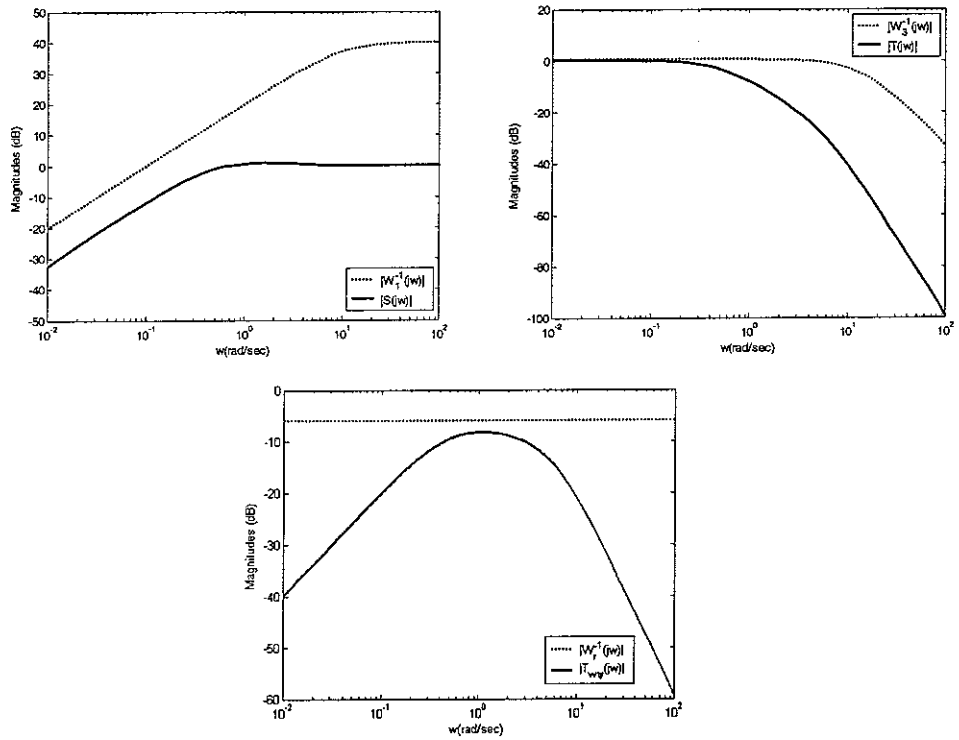

Figure 6. Frequency responses of closed-loop heading control system
Upper left: the sensitivity function, upper right: the complementary sensitivity function, bottom: the yaw rate

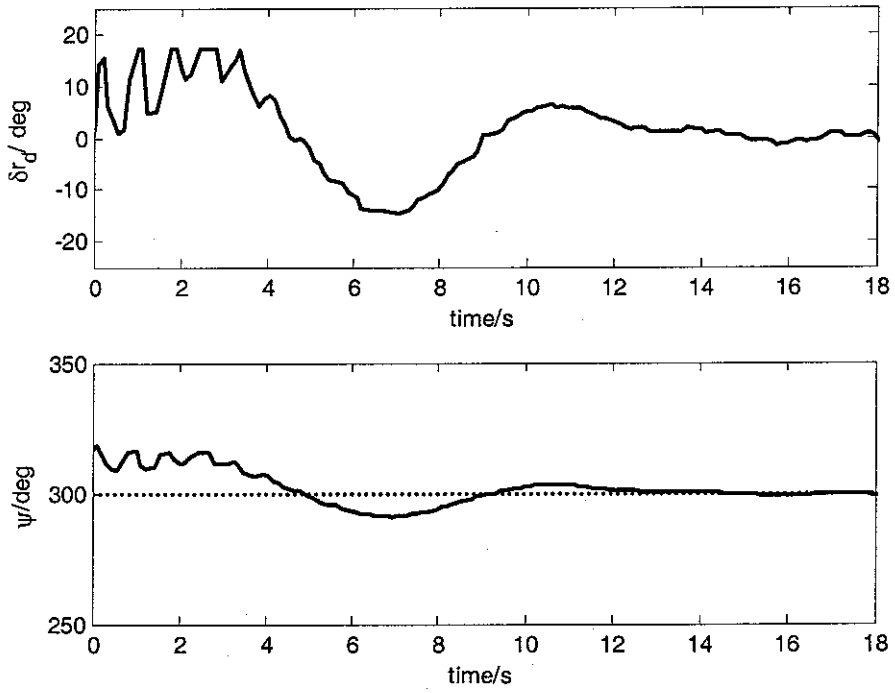

Figure 7. Test result of heading control.
Upper: rudder command, bottom: actual heading (solid) and demanded heading (dotted)

4 Redesign of longitudinal autopilot

In the old design, the forward speed and depth of the vehicle were controlled by a single MIMO controller-the longitudinal autopilot. Although the non-linear simulation results demonstrated the effectiveness of the autopilot, it was found from real tests the tracking performance of depth is very poor. The vehicle cannot maintain a set depth even after it had travelled a distance of about 20m.

The main reason for this is believed to be the model uncertainty. Since the longitudinal autopilot was designed for the nominal operating point, it is no doubt that the performance will degrade when the autopilot is applied under off-nominal operation conditions. In our case, the autopilot was designed for the cruise control, but it was working in a wide speed range where the vehicle accelerated from stationary to a set speed that may be not the cruise speed.

Therefore it is necessary to improve the performance of the longitudinal autopilot, especially in the depth tracking. To improve the tracking performance, a common sense approach is to introduce the rate of the output, if available, to the feedback channel.

For underwater vehicles, the depth rate can be described by

$$\dot{z} = -u\sin\theta + v\sin\phi\cos\theta + w\cos\phi\cos\theta$$

Due to the passive stability of the roll modes and the negligible heave speed for an underwater flight vehicle, the depth rate around the cruise condition can be simplified by

$$\dot{z} \approx -u_0\theta \tag{25}$$

where u_0 is the cruise speed (1.3m/s). Therefore the pitch angle reflects the depth rate for an underwater flight vehicle; this suggests the introduction of the pitch angle to feedback control of depth. Fortunately the digital compass onboard Subzero III provides reliable attitude angles.

As for the speed control, since the forward acceleration provided by the axial accelerometer is too noisy to be useful for feedback control, only output will be fed back.

Therefore, in the new design the longitudinal control will be achieved by two sub-controllers i.e. the speed autopilot and the depth autopilot. While the former is a SISO controller, the latter is a MISO controller.

4.1 Redesign of the speed autopilot

Select the state, control input and output vectors as

$$x_G = [u, n]^T, u_G = m_d, y_G = u$$

The state space model of the speed system around cruise condition is

$$G(s) = \left[\begin{array}{c|c} A_G & B_G \\ \hline C_G & D_G \end{array}\right] = \left[\begin{array}{cc|c} -0.554 & 0.05818 & 0 \\ 7.20 & -4.08 & 0.0492 \\ \hline 1 & 0 & 0 \end{array}\right] \tag{26}$$

In terms of the saturation limit of the propeller command, the weighting function $W_2(s)$ (cf. Figure 1) is selected as

$$W_2(s) = W_2 = 1/2500 \tag{27}$$

The remaining weighting functions are the same as (7) and (9).

By inserting the plant model (26), the weighting functions (7),(9) and (27) into (18), a generalized plant model of 3rd order can be obtained. Substituting this model into (1), and invoking the design procedure for synthesizing a reduced-order H_∞ controller, a second order autopilot with H_∞ performance of 0.9997 can be obtained. The transfer function of the speed autopilot is

$$K_u(s) = \frac{381.025(s+5.031)(s+0.4795)}{(s+2.298)(s+0.0005713)} \tag{28}$$

The frequency responses of the sensitivity function, the complementary sensitivity function and the control effort function are shown in Figure 8. It can be seen that the design specifications are met.

4.2 Redesign of the depth autopilot

Selecting the state, control input and output vectors as

$$x_\theta = [\theta, w, q, \delta s]^T, u_\theta = \delta s_d, y_\theta = \theta$$

and linearizing the non-linear model Subzero III around the cruise condition yields the state space model of the pitch angle as follows

$$G_\theta(s) = \left[\begin{array}{c|c} A_\theta & B_\theta \\ \hline C_\theta & D_\theta \end{array}\right] = \left[\begin{array}{cccc|c} 0 & 0 & 1 & 0 & 0 \\ -0.01746 & -2.124 & -0.3732 & -0.3294 & 0 \\ -0.6474 & -7.991 & -8.701 & -2.431 & 0 \\ 0 & 0 & 0 & -11.53 & 1 \\ \hline 1 & 0 & 0 & 0 & 0 \end{array}\right] \tag{29}$$

Since the heave speed of an underwater flight vehicle is quite small, it can be removed from the state space model (28). Thus the reduced model is

$$G_\theta(s) = \left[\begin{array}{c|c} A_\theta & B_\theta \\ \hline C_\theta & D_\theta \end{array}\right] \approx \left[\begin{array}{ccc|c} 0 & 1 & 0 & 0 \\ -0.6474 & -8.701 & -2.431 & 0 \\ 0 & 0 & -11.53 & 1 \\ \hline 1 & 0 & 0 & 0 \end{array}\right] \tag{30}$$

Recalling (25), the transfer function of the depth system is

$$G(s) \approx -\frac{u_0}{s} G_\theta(s) \tag{31}$$

As stated earlier, the new depth autopilot is a MISO controller. The robust depth control system is depicted in Figure 9. The depth autopilot (enclosed by the dashed lines) has the depth error e_z and the pitch angle θ as its input, and has the stern-planes command δs_d as its output.

As shown in Figure 9, unlike a typical mixed sensitivity optimisation frame, the pitch angle instead of the stern-plane is penalized. There are two reasons for this modification.

The first reason is it can avoid the conservativeness caused by penalizing the stern-plane command. Due to the dynamics of the servomechanism of the stern-plane, to confine its effort (position) is not the same as to restrict its command. In other words, the stern-plane's position is always less than the corresponding command. Therefore restricting the stern-plane command is only an indirect and conservative way for confining control effort. Since the pitch angle directly reflects the deflection of the stern-plane, penalizing it is a desirable choice for restricting the control effort.

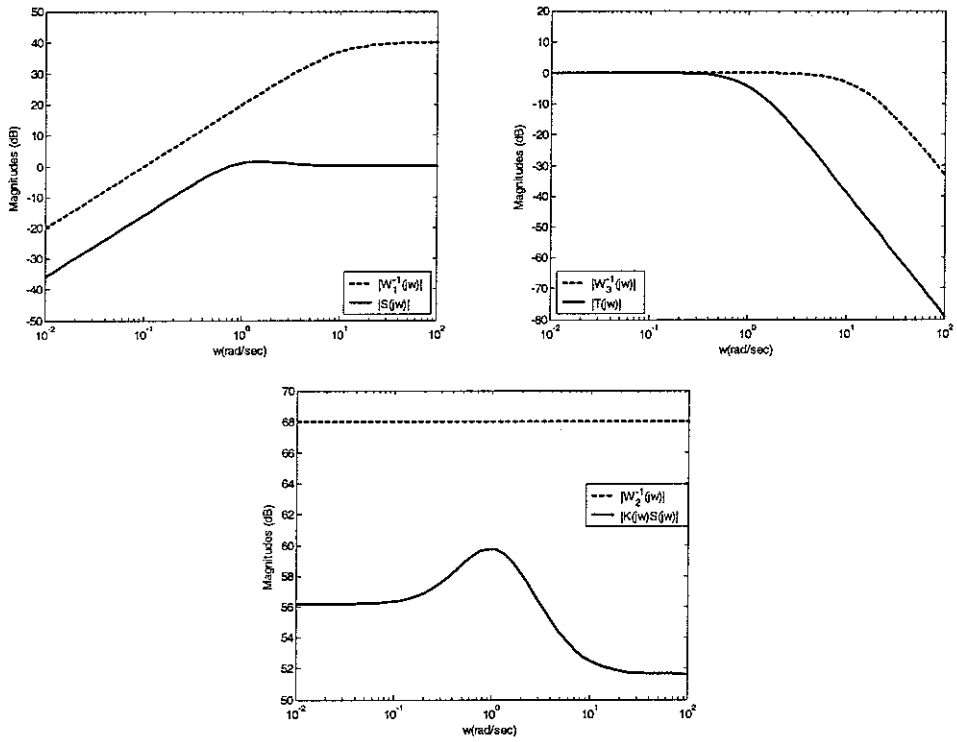

Figure 8. Frequency responses of closed-loop speed control system
Upper left: the sensitivity function, upper right: the complementary sensitivity function, bottom: the control effort

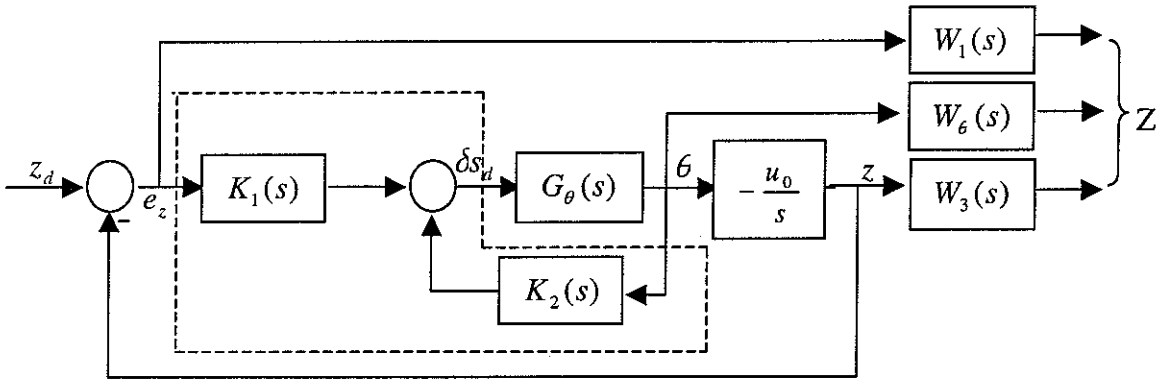

Figure 9. The robust depth control system

The second reason is it can avoid the representation singularity of the Euler angles. It is a well known fact the vehicle's attitude cannot be described by the Euler angles when the pitch angle is close to ±90 degrees. In our case, the digital compass can only provide reliable attitude angles within a tilt of 50 degrees. Restricting the pitch angle provides a direct way to avoid this phenomenon.

Since the depth of the Lamont Tank is about 1m, here the weighting function $W_\theta(s)$ is selected as

$$W_\theta(s) = W_\theta = \frac{6}{\pi} \tag{32}$$

This implies that for a one-meter step depth demand, the absolute value of pitch angle needs to be less than 30 degrees.

The remaining weighting functions $W_1(s)$ and $W_3(s)$ are the same as those in (7) and (9).

By setting δs_d as the control input, (e_z, θ) as the measurement, z_d as the external input, and Z as the controlled output, the generalized plant can be obtained.

$$P(s)=\left[\begin{array}{c|c} W_1(s) & -W_3(s)G(s) \\ 0 & W_\theta(s)G_\theta(s) \\ 0 & W_3(s)G(s) \\ \hline I & -G(s) \\ 0 & G_\theta(s) \end{array}\right], G(s)=-\frac{u_0}{s}G_\theta(s), K(s)=\begin{bmatrix} K_1(s) & K_2(s) \end{bmatrix} \quad (33)$$

The minimal realization is

$$\left[\begin{array}{c|c|c} A & B_1 & B_2 \\ \hline C_1 & D_{11} & D_{12} \\ \hline C_2 & D_{21} & D_{22} \end{array}\right] =$$

$$\left[\begin{array}{ccc|c|c} A_{W_1} & -B_{W_1} & 0 & B_{W_1} & 0 \\ 0 & 0 & -u_0C_\theta & 0 & -u_0D_\theta \\ 0 & 0 & A_\theta & 0 & B_\theta \\ \hline C_{W_1} & -D_{W_1} & 0 & D_{W_1} & 0 \\ 0 & 0 & W_\theta C_\theta & 0 & W_\theta D_\theta \\ 0 & \Pi_0 & -u_0(\Pi_1 C_\theta + \Pi_2 C_\theta A_\theta) & 0 & -u_0(\Pi_1 D_\theta + \Pi_2 C_\theta B_\theta) \\ \hline 0 & -1 & 0 & 1 & 0 \\ 0 & 0 & C_\theta & 0 & D_\theta \end{array}\right] \quad (34)$$

Substituting (34) into (1), and applying the approach for synthesizing the reduced-order H_∞ controller yields a second order controller with H_∞ performance of 0.9964. The transfer function of the depth autopilot is

$$K_z(s)=\left[\frac{6.4538(s+12.99)(s+0.006654)}{(s+4.049)(s+0.0008881)} \quad \frac{26.1033(s+9.359)(s+0.0003794)}{(s+4.049)(s+0.0008881)}\right] \quad (35)$$

The frequency responses of the sensitivity function and the complementary sensitivity function of the closed-loop depth control system and the closed-loop pitch angle system are shown in Figure 10.

The vehicle was equipped with the longitudinal autopilot (28) and (35), and tested in the Lamont Tank. It was found that the performance of the longitudinal control of Subzero III is desirable. A test result is shown in Figure 11. From Figure 11, it can be seen while the speed control system has no steady state error, the depth control system has an acceptable steady state error. This error is mainly caused by the offset of the stern-panes from their central positions. Although the compensation for the offset has been included in the control software, it is unlikely to remove the offsets completely.

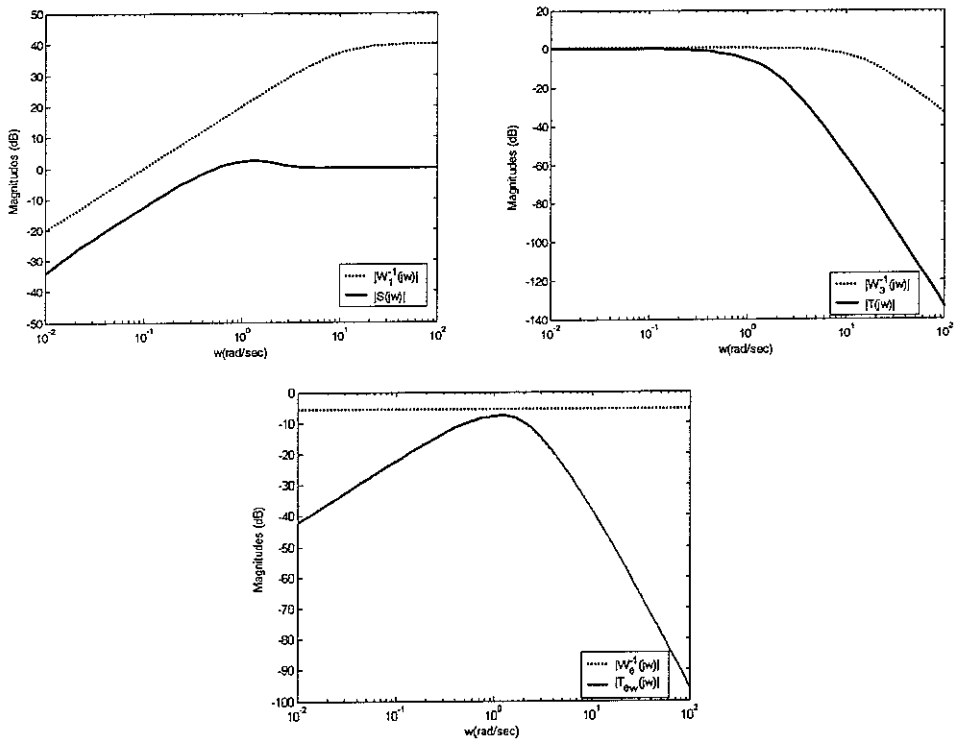

Figure 10. Frequency responses of closed-loop speed control system
Upper left: the sensitivity function, upper right: the complementary sensitivity function, bottom: the control effort

5 Conclusions

This report presents the redesign of the autopilots for the flight control of Subzero III in the restricted water of the Lamont Tank. All the autopilots are reduced-order H_∞ controllers.

Real water tests show the effectiveness of the autopilots since the vehicle equipped with the heading autopilot and the longitudinal autopilot has desirable tracking performance and acceptable overshoots in the heading and depth which are critical for the restricted water.

Moreover, although the autopilots are designed for the cruise condition, it is seen via water trails that they worked well under the off-nominal conditions i.e. the vehicle accelerated from stationary to a desired speed i.e. 1m/s. Therefore only a single fixed-parameter controller is needed for the flight control of Subzero III for the speed range from 0 to its cruise speed or even higher. This indicates the robustness of the autopilots to the model uncertainty.

In the near future the new autopilots, as well as the old autopilots presented in previous reports, will be tried in open water where underwater currents may be present. That is to say the robustness of the autopilots to external disturbances will be checked.

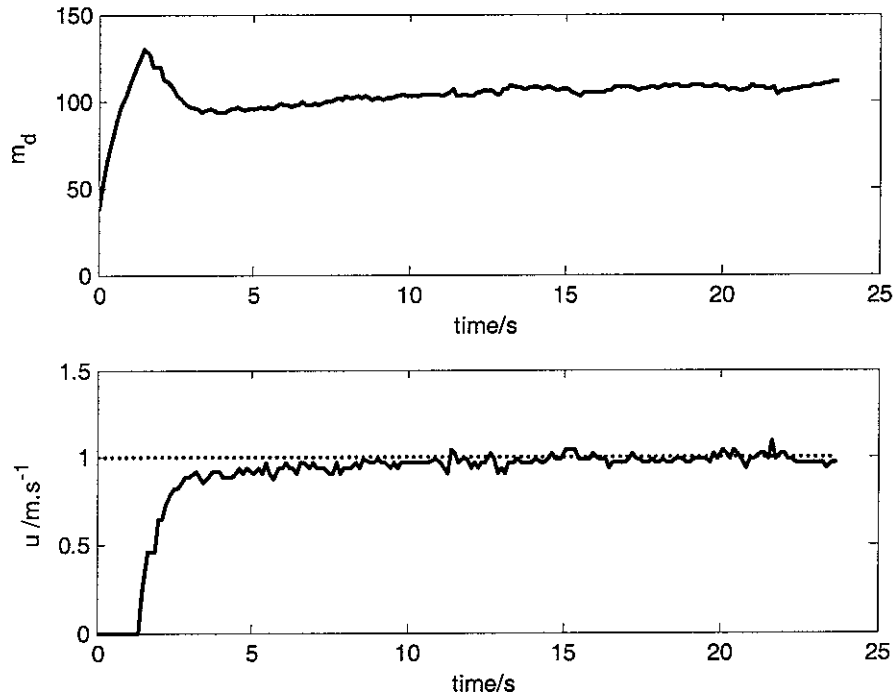

(a) Test result of forward speed control
Upper: propeller command, bottom: actual (solid) and demanded (dashed) forward speed

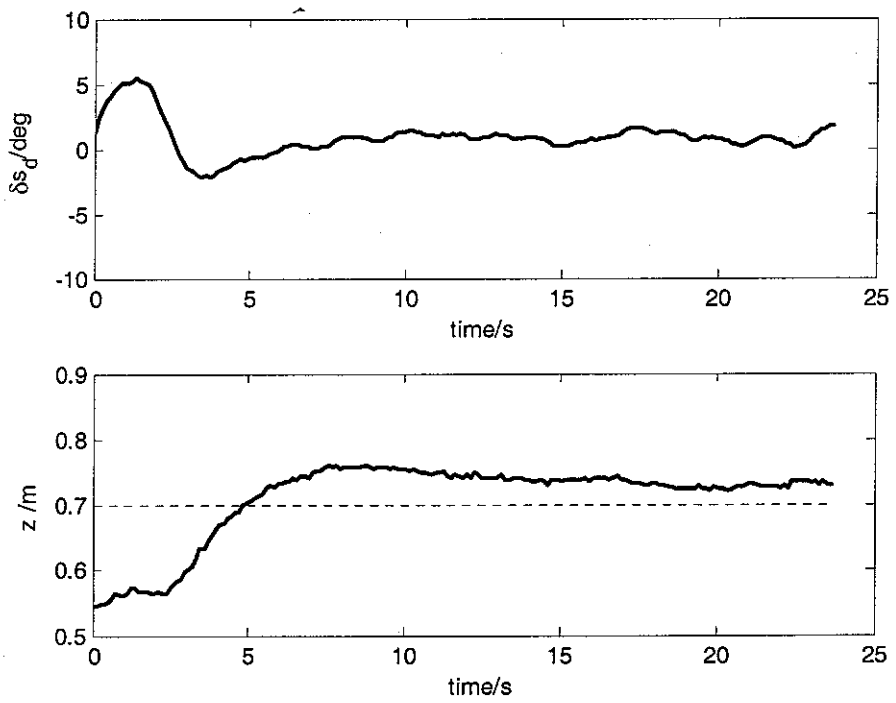

(b) Test result of depth control
Upper: stern-plane command, bottom: actual (solid) and demanded (dashed) depth
Figure 11. Test results of longitudinal control

References

El Ghaoui, L. and P. Gahinet (1993). Rank minimization under LMI constraints: A framework for Output Feedback

Problems. *Proc. European Control Conference.*

Fazel, M. (2002). Matrix Rank Minimization with Applications. PhD Thesis, Stanford University, March 2002.

Gahinet,P. and P. Apkarian (1994). A linear matrix inequality approach to H_∞ control. *Int. J. Robust Nonlinear Control*, **4**,421-448.

Hu, J., C. Bohn and H.R. Wu (2000). Systematic H_∞ weighting function selection and its application to the real-time control of a vertical take-off aircraft. *Control Engineering Practice 8(3): 241-252*

Iwasaki, T. and R. E. Skelton (1994). All controllers for the general H_∞ control problem: LMI existence conditions and state space formulas. *Automatica, 30(8):1307-1317.*

Pare, T. E. and J. P. How(1999). Algorithms for Reduced Order Robust H_∞ Control Design. *Proc. IEEE CDC, pp1863-1868*

Feng, Z. and R. Allen (2002a). Design of Subzero II H_∞ Autopilot, IMPROVES report, January 2002

Feng, Z. and R. Allen (2002b). Reduced-order H_∞ Autopilot Design for Subzero II, IMPROVES report, November 2002